

Attention2Minority: A salient instance inference-based multiple instance learning for classifying small lesions in whole slide images

Ziyu Su, Mostafa Rezapour, Usama Sajjad, Metin Nafi Gurcan, Muhammad Khalid Khan Niazi

Abstract— Multiple instance learning (MIL) models have achieved remarkable success in analyzing whole slide images (WSIs) for disease classification problems. However, with regard to gigapixel WSI classification problems, current MIL models are often incapable of differentiating a WSI with extremely small tumor lesions. This minute tumor-to-normal area ratio in a MIL bag inhibits the attention mechanism from properly weighting the areas corresponding to minor tumor lesions. To overcome this challenge, we propose salient instance inference MIL (SiiMIL), a weakly-supervised MIL model for WSI classification. Our method initially learns representations of normal WSIs, and it then compares the normal WSIs representations with all the input patches to infer the salient instances of the input WSI. Finally, it employs attention-based MIL to perform the slide-level classification based on the selected patches of the WSI. Our experiments imply that SiiMIL can accurately identify tumor instances, which could only take up less than 1% of a WSI, so that the ratio of tumor to normal instances within a bag can increase by two to four times. It is worth mentioning that it performs equally well for large tumor lesions. As a result, SiiMIL achieves a significant improvement in performance over the state-of-the-art MIL methods.

Index Terms— Deep Learning, Whole Slide Image Analysis, Multiple Instance Learning, Weakly Supervised Classification

1 INTRODUCTION

HISTOPATHOLOGY plays a crucial role in clinical diagnosis and is widely used as a diagnostic tool for multiple diseases [1]. In addition, with the fast development in digital scanning, data storage and data transmission technologies, whole slide image (WSI) technology has made histopathological slides more accessible and easier to analyze [2]. WSIs usually have gigapixel-level resolution that enables pathologists to see details of the biological tissues in high magnification. This sheer size of WSI, on the other hand, makes manual delineation and diagnosis/prognosis difficult and time-consuming. As a result, there is a growing interest in developing automated methods for mining diagnostic and predictive information from WSIs.

Deep learning is a supervised-learning paradigm in which the term "deep" refers to a neural network's numerous hidden layers. Deep learning-based medical image analysis techniques have advanced significantly during the last decade [3]. As a result, deep learning is the common choice for the automatic WSI analysis, showing substantial advancements over earlier approaches [4-7]. However, fully supervised-deep learning models cannot

be used for many pathology problems since they require laborious and time-consuming fine-grained annotations. As a result, weakly supervised learning, a paradigm in which the model just needs to be trained using WSI-level diagnostic labels, has risen in prominence in recent years [8-10]. Multiple instance learning (MIL) is one of the most extensively used weakly supervised learning methods for WSIs [11, 12]. In MIL, high-resolution WSIs are divided into smaller patches, then the information extracted from these patches is combined to make slide-level predictions or classifications.

Some MIL models use neural networks to learn attention weights for each patch of the WSI. These weights can be visualized to learn which parts of the WSI are prioritized by the MIL model when making a decision [9, 10, 12, 13]. However, for early diagnosis, the WSI-level labels frequently correspond to exceedingly small lesions (limited to a few patches) in the WSIs, which sometimes account for a very small (typically less than 1%) portion of the total WSIs. As patch data contains a limited amount of meaningful information (patches corresponding to the

• The authors are with the Center for Biomedical Informatics, Wake Forest University School of Medicine, Winston-Salem, NC 27101. E-mail: zsu@wakehealth.edu

(Corresponding author: Ziyu Su)

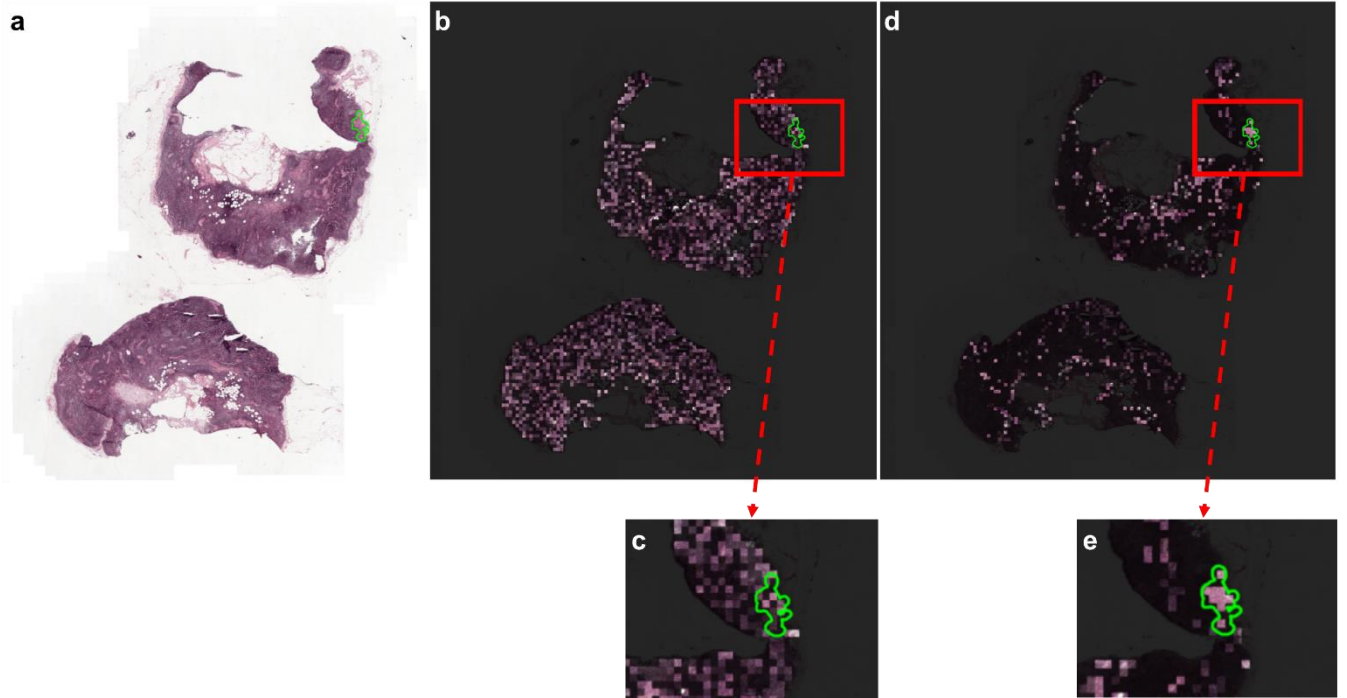


Fig. 1. Comparison of attention heatmaps for a tumor WSI produced by a current attention-based model and the proposed SiiMIL model. The heatmaps are visualized by overlaying the attention weights to the corresponding local regions of the WSI. Tumors are annotated in green. (a) Original tumor WSI with tumor annotation. (b) Attention heatmaps produced by an attention-based model. (c) Magnified local region. (d) Attention heatmaps produced by the proposed SiiMIL. (e) Magnified local region. From (b) and (c), we observe that the attention-based model fails to pay higher attention to the tumor region. In contrast, the proposed SiiMIL pays higher attention to the tumor region and pays relatively low attention to the non-tumor region.

small lesion), the MIL models fail to pay attention to the small lesion during the analysis. This effect is illustrated in Fig. 1a, b and c, where we overlaid the MIL model [12] generated attention weights over a tumor WSI. Other MIL models attempt to only feed partially important regions of the WSIs to the deep learning models to highlight the important regions of the WSIs [8, 14-16]. In these models, the essential idea is to train a patch selection network using the WSI-level labels and then select a few patches as the representation of the WSI. This kind of methodology works better in situations where the WSIs have predominant regions that correspond to the WSI label, such as cancer subtyping, Gleason grading, and tissue regeneration grading problems [16]. However, these approaches may fail for WSI with small lesions since most of the patches do not correspond to a slide label. Expecting a patch selection network to uncover these minority patches is akin to looking for a needle in a haystack. Given these difficulties, a robust patch selection technique for the MIL models is critical.

Here, we propose a novel MIL model named salient instance inference MIL (SiiMIL) and its application to classification of breast cancer metastasis to lymph node, i.e., tumor vs. normal classification. In the proposed model, we first learn a set of representative normal patches from the normal WSIs. Then, we creatively infer the possible lesion patches of an input WSI by comparing the similarities between all the input patches and a set of representative

normal patches. Finally, we aggregate the inferred patches and make a prediction using a deep-learning model. In our patch inferring method, we avoid training with noisy labels (patches that are predominant and do not correspond to the WSI label) because we do not rely on any tumor WSIs. To determine the salient instances, our model takes advantage of the fact that each patch in a normal WSI corresponds to the WSI label. So, it only uses patches from normal WSIs during the determination of salient instances. In other words, similar to open-world learning, our model learns to recognize normal representation while treating the tumor patches as an unknown class [17].

2 MATERIALS AND METHODS

2.1 Dataset

Our study is developed based on the Camelyon16 dataset [18]. Camelyon16 is a publicly available WSI dataset for breast cancer lymph node metastases classification. The training set includes 271 WSIs, and the hold-out testing set has 129 WSIs divided into two classes: normal and tumor. In this weakly supervised learning study, only the WSI-level labels (i.e., normal or tumor) are available.

2.2 Multiple instance learning for WSI classification

In MIL formulation, a bag refers to the set of unlabeled instances in a WSI. Each bag's label is determined by the

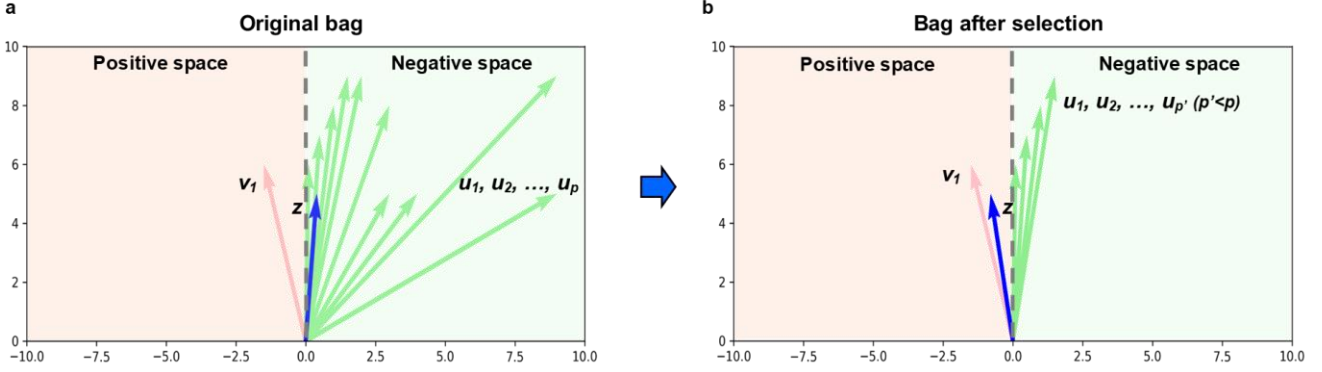


Fig. 2. Justification of salient instance inference in a 2-D example. (a) We show a 2-D example of MIL aggregation for a small tumor WSI when all instances are used for aggregation. The red arrow indicates the positive instance v_1 , green arrows indicate the negative instances $u_{1,2,\dots,p}$, and the blue arrow indicates the combined bag-level representation z . (b) By selecting salient instances and omitting some easily recognizable negative instances, we reduce the number of negative instances from p to p' , where $p' < p$. Thus, the bag-level representation z will fall back to the positive space.

presence of positive instances. In other words, a positive bag needs to contain at least one positive instance and a negative bag needs to exclusively contain negative instances. Therefore, we formulate the MIL problem as:

$$Y = \begin{cases} 0, & \text{iff } \sum_i y_i = 0, \\ 1, & \text{otherwise.} \end{cases} \quad (1)$$

where Y is the label of the bag and $y_i \in \{0, 1\}$, for $i = 1, \dots, m$, is the label of instance inside the bag [11]. To predict the bag-level label Y , the MIL models need to analyze and aggregate the instances, and then reach the conclusion in the form of:

$$Y = g(\sigma(f(x_1), \dots, f(x_m))) \quad (2)$$

where $f(\cdot)$ is the feature extraction function for instances, $\sigma(\cdot)$ is the aggregation operator, and $g(\cdot)$ is the bag-level classifier.

For a variety of reasons, the WSI classification inevitably develops into the MIL formulation. First, the raw images of WSIs with gigapixel resolution seldom fit in the available graphics processor memory. As a result, the typical paradigm entails cropping a WSI into numerous image patches and then extracting feature embeddings from the patches using a feature extractor (i.e., the $f(\cdot)$ function). This enables us to fit all embedding into a GPU memory. Second, in WSI classification, such as normal/tumor, bags containing embeddings from lesion areas might be deemed positive because they are only present in tumor WSIs. Third, as it is painstakingly difficult to annotate WSIs, we often have access to the WSI-level labels (i.e., Y) but not the instance-level labels (i.e., y_i). The ability of MIL to address all three problems makes it a suitable candidate for WSI-level classification.

In the case of tumor WSI with small lesions, the WSIs typically contain dominant regions of normal tissues, making it difficult for the MIL model to focus on the patches corresponding to small lesions [13]. For instance, in Camelyon16 dataset, the ratio of tumor region to the

entire tissue region of a tumor WSI could be lower than 0.5%.

2.3 Motivation of salient instance inference

To depict the motivation of our method, we take tumor WSIs classification as an example. Consider a tumor WSI (positive bag) with a small number of tumor patch feature embeddings (positive instances). Let $\{u_1, u_2, \dots, u_p, v_1, v_2, \dots, v_q\}$ denote $m = p + q$ instances of the WSI, where $u_i \in \mathbb{R}^D$ and $v_j \in \mathbb{R}^D$, for $i = 1, 2, \dots, p$ and $j = 1, 2, \dots, q$, denote the negative and positive instances, respectively. For the WSI with small lesions, we assume that $p \gg q$.

Assuming that our MIL aggregation function is weighted average:

$$z = \sum_{i=1}^p a_i u_i + \sum_{j=1}^q b_j v_j \quad (3)$$

where $z \in \mathbb{R}^D$ is the bag-level representation and a_i and $b_j \in \mathbb{R}$ for $i = 1, 2, \dots, p$ and $j = 1, 2, \dots, q$ are the weights emphasizing the positive instances and $\sum_{i=1}^p a_i + \sum_{j=1}^q b_j = 1$. In other words, the bag-level representation is a convex combination of all negative and positive instances in a bag. Considering the morphological difference between tumor and normal tissues, the positive and negative instances should lay in different sub-spaces. However, since $p \gg q$, if the attention scores of the negative instances are not sufficiently small, the resulting convex combination z will easily fall into the negative subspace. As a result, the positive bag-level representation will be inseparable from the negative bag. This effect is demonstrated in Section 3.1. On the other hand, if we intentionally select possible positive instances in the bag, therefore increasing the density of positive instances in the positive bags, we can make the bag-level representation more separable from the negative bag and derive an easier classification problem. Please see Fig. 2 as a toy example when the instance dimension $D = 2$.

For a naïve solution, if we can have an accurate instance-level positive instance prediction model, we can easily select high probability instances to achieve our goal. However, this type of prediction model usually requires fully supervised training with reliable instance labels, which is impossible for most WSI classification cases. Therefore, a weakly supervised patch selection methodology is crucial to tackling the MIL problem.

2.4 Salient instance inference

Our salient instance inference (Sii) is composed of the following three steps: (i) learning representative instances from negative (normal) WSIs in the training set; (ii) comparing similarities between the instances of an input WSI and the learned representative instances; (iii) selecting instances with low similarity scores (i.e., high saliency) from the input WSI to form a bag.

2.4.1 Motivation for key instance selection through representation learning

As there is anatomical redundancy among normal histopathological slides, we are interested in identifying a subset of negative instances that can represent all normal instances. We call this subset as a set of representative negative instances. The primary idea is to use these negative instances to find instances in an input WSI that are least similar to negative instances. Our reasons for doing this are threefold. As negative and positive instances have different patterns in image and feature space, there is a high likelihood that the instances that are the least similar to the representative negative instances are positive instances. Second, in a normal WSI, we can assign each negative instance with the same label as the WSI. In other words, each negative instance in normal WSIs can be deemed absolutely normal. As a result, fine annotation by pathologists is not needed for normal WSIs. Finally, we have an abundance of negative examples (resulting from normal WSIs) to reliably identify representative negative instances. We use the CUR decomposition to learn representative negative instances from the negative instances [19].

For large datasets consisting of m objects, each of which is described by n features, can be encoded as a matrix $A \in \mathbb{R}^{m \times n}$ with m rows (objects) and n columns (features). Hence, to reduce computational costs related to large datasets, we can find ways to deal with large matrices instead of large datasets. During the past quarter century, different matrix decomposition methods have been studied and used to construct low-rank matrix approximations. For instance, Singular Value Decomposition (SVD) is one of the most widely used matrix decomposition methods that compress data into its fundamental features that are necessary for understanding, describing, and analyzing data. When it comes to dealing with high-throughput data, SVD is often the first phase of data analytics and machine learning. In general, SVD decomposes a large $m \times n$ matrix into a left singular vector, diagonal singular value matrix, and right singular value matrix. SVD utilizes the eigenvalues and corresponding unit ei-

genvectors to compute a decomposition in the form of $A = U\Sigma V^T$. However, in many cases, the matrices U and V lack physical meaning and are hard to interpret because they store merely eigenvectors corresponding to the singular values. This property makes it especially inefficient in our task since we prefer comparing actual feature embeddings with each other instead of comparing eigenvectors with feature embeddings. To solve this problem, other forms of matrix decomposition have been introduced that are interpretable such as CUR decomposition.

The CUR decomposition technique finds a small number of representable rows or/and columns from a matrix $A \in \mathbb{R}^{m \times n}$ to form an interpretable compressed representation of the matrix. The CUR decomposition forms a matrix $C \in \mathbb{R}^{m \times c}$ with a small number (i.e., $c \leq n$) of columns from matrix A , and a matrix $R \in \mathbb{R}^{r \times n}$ with a small number (i.e., $r \leq m$) of rows from matrix A . Finally, given a rank parameter $k \leq \text{rank}(A)$ and an error parameter $\varepsilon > 0$, a matrix $U \in \mathbb{R}^{c \times r}$ is constructed such that the approximation $A' = CUR$ is relatively close to A , i.e., $CUR \approx A$. We often seek an approximation A' whose relative-matrix error using Frobenius norm satisfies $\|A - A'\|_F \leq (1 + \varepsilon)\|A - A_k\|_F$, where A_k is the best rank- k approximation provided by the truncated SVD of A while c, r , and $\text{rank}(U)$ being as small as possible [19, 20].

The CUR decomposition forms a low-rank approximation to an $m \times n$ matrix A that has a straightforward interpretation and preserves important properties of A , such as sparsity and non-negativity. Many methods have been introduced to construct C, R , and U efficiently, but Drineas et al. [20] and Mahoney et al. [19] introduced two effective methods for selecting the most informative columns of A . Drineas et al. [20] used subspace sampling to construct a non-uniform probability distribution from a small sample of columns. Subspace sampling allows one to entirely represent a specified subspace of interest. Their algorithm works in a two-stage process. The first stage of the algorithm involves a standard column selection procedure of A . Then, the second stage solves a column selection process on the transpose of A . Their method was the first to achieve relative error instead of additive error. In addition, their algorithm had a running time of $O(mnk)$, which is dominated by the running time of the truncated SVD of A . Given a matrix $A \in \mathbb{R}^{m \times n}$, Mahoney et al. [19] used statistical leveraging to compute a CUR matrix decomposition of A . To find matrices C and R , they computed an importance score for each row and column in A . The importance score is the statistical leverage or influence of each row and column in A on its optimal low-rank approximation. Rows and columns with high leverage scores have high statistical significance and are important to include in the matrix decomposition. Using the normalized leverage formula, they found a representation for C and R based on existing columns and rows in A .

2.4.2 Representation learning from negative instances

Let $X = \{X_1, X_2, \dots, X_p\}$ denotes all normal WSIs in our training set, and $X_i = \{x_{i1}, x_{i2}, \dots, x_{in_i}\}$ denotes all image patches inside the WSI X_i , where $i = 1, \dots, n_i$ and n_i is dependent on the size of the tissue inside the WSI. We first

apply a feature extraction neural network $f(\cdot)$ to embed x_{ij} to feature embedding $h_{ij} = f(x_{ij}) \in \mathbb{R}^D$, where $i = 1, 2, \dots, P$ and $j = 1, 2, \dots, n_i$. Thus, for each WSI X_i , we have a matrix of feature embeddings $A_i = [h_{i1}, h_{i2}, \dots, h_{in_i}] \in \mathbb{R}^{D \times n_i}$.

Given a normal WSI with feature embeddings $A_i \in \mathbb{R}^{D \times n_i}$, if $n_i \gg D$, then there might exist $t_i \ll n_i$ feature embeddings that contain sufficient information to represent the WSI. To find out the t_i most representative feature embeddings, we first apply the CUR decomposition to A_i to construct a low-rank matrix approximation $\tilde{A}_i \in \mathbb{R}^{D \times t_i}$, for $i = 1, 2, \dots, P$ as follows:

- Step 1. Compute the rank of A_i , and set $k = \text{rank}(A_i)$.
- Step 2. Construct matrix V whose rows are the eigenvectors of $A_i^T A_i$.
- Step 3. Compute the importance score of the j^{th} column of A_i by

$$s_j = \frac{1}{k} \sum_{h=1}^k V_{hj}^2 \quad (4)$$

where V_{hj} is the element in the h^{th} row and j^{th} column of V , for $j = 1, 2, \dots, n_i$.

- Step 4. Sort columns of A_{b_i} based on the scores s_j 's.
- Step 5. Construct $\tilde{A}_{b_i} \in \mathbb{R}^{D \times t_i}$ whose columns are the first t_i columns of sorted A_{b_i} in Step 4.

We then construct a key matrix K by concatenating all \tilde{A}_{b_i} for $i = 1, 2, \dots, P$,

$$K = \tilde{A}_{b_1} \oplus \tilde{A}_{b_2} \dots \oplus \tilde{A}_{b_P} = [k_1, \dots, k_\tau] \in \mathbb{R}^{D \times \tau} \quad (5)$$

where \oplus denotes the concatenation operation and $\tau = \sum_{i=1}^P t_i$, and each column $k_j \in \mathbb{R}^D$, for $j = 1, 2, \dots, \tau$, is a representative negative instance.

2.4.3 Bag generation

In this stage, for each WSI, we select salient instances to form a bag. Given all instances inside an input WSI, we think that the instances that are dissimilar to the representative negative instances (see 3.4.2) are with high saliency and should be included in the bag for the input WSI. In other words, we keep the instances that are more likely to be lesions and remove those simple-recognizable “normal” instances in the bag. As a result, we can yield a bag with a higher positive instance rate that is easily separable from the normal bag. We name this procedure salient instance inference (Sii). Please note that applying Sii on a normal WSI will not significantly affect the classification since the remaining instances of a negative bag will still be negative.

In detail, let $Q = [q_1, \dots, q_n] \in \mathbb{R}^{D \times n}$ denotes the matrix of all instances of an input WSI where each column q_i is an instance (i.e. patch embedding) of the WSI and $K = [k_1, \dots, k_\tau] \in \mathbb{R}^{D \times \tau}$ denotes the representative negative instances from last stage. Inspired by the transformer model [21], we refer q_i as queries and k_j as keys. We build

a cross similarity matrix $C \in \mathbb{R}^{m \times n}$ where each entry is the cosine similarity of a (q_i, k_j) pair:

$$C_{ij} = \frac{q_i^T k_j}{\|q_i\| \|k_j\|}, \quad i = 1, \dots, n, \quad j = 1, \dots, \tau \quad (6)$$

Then, for each query q_i , we define its saliency score $s_i \in \mathbb{R}$ as:

$$s_i = -\text{Avg}(\text{Top}K(C_{ij}))_{j=1, \dots, \tau} \quad (7)$$

where $\text{Top}K$ operator denote finding the top- K highest C_{ij} along the j axis of the matrix C . Specifically, we are finding the K nearest neighbors from all the keys for each query and then take the average of the corresponding similarity values. Since we define low similarity values as high saliencies, we take the negative average operation to produce the final saliency score s_i for q_i .

Finally, we infer the salient query instances by selecting the queries with top- $r\%$ saliency score, where $r \in [0, 1]$ is a percentage number and form the bag $B = \{q_1, \dots, q_t\}$, where $t = r \cdot n$, for this WSI using these query instances.

The processing steps of the completed Sii is depicted in Algorithm 1.

Algorithm 1 Salient instance inference (Sii)

Part 1. Representation learning from negative instances:

Input: The set of normal WSIs, $X = \{X_1, X_2, \dots, X_P\}$.

Step 1: for $i = 1, 2, \dots, P$ do

- **Step 1.1:** Compute the rank of A_i , and set $k = \text{rank}(A_i)$.
- **Step 1.2:** Construct matrix V whose rows are the eigenvectors of $A_i^T A_i$.
- **Step 1.3:** Compute the importance score of the j^{th} column of A_i by $s_j = \frac{1}{k} \sum_{h=1}^k V_{hj}^2$, where V_{hj} is the element in the h^{th} row and j^{th} column of V , for $j = 1, 2, \dots, n_i$.
- **Step 1.4:** Sort columns of A_{b_i} based on the scores s_j 's.
- **Step 1.5:** Construct $\tilde{A}_{b_i} \in \mathbb{R}^{D \times t_i}$ whose columns are the first t_i columns of sorted A_{b_i} in Step 1.4.

End (for).

Output: Construct a key matrix K by concatenating all \tilde{A}_{b_i} , for $i = 1, 2, \dots, P$,

$$K = \tilde{A}_{b_1} \oplus \tilde{A}_{b_2} \dots \oplus \tilde{A}_{b_P} = [k_1, \dots, k_\tau] \in \mathbb{R}^{D \times \tau}.$$

Part 2. Bag generation:

Input:

- The key matrix K obtained in **Part 1**.
- All patch embeddings from a WSI (normal or tumor).

Step 1: Compute $C = \tilde{Q}^T \tilde{K}$, where

$$\tilde{Q} = \left[\frac{q_1}{\|q_1\|}, \frac{q_2}{\|q_2\|}, \dots, \frac{q_n}{\|q_n\|} \right] \text{ and } \tilde{K} = \left[\frac{k_1}{\|k_1\|}, \frac{k_2}{\|k_2\|}, \dots, \frac{k_\tau}{\|k_\tau\|} \right].$$

Step 2: Compute $S = [s_i]_{n \times 1}$, where $s_i = -\text{Avg}(\text{Top}K(C_{ij}))_{j=1, \dots, \tau}$ and c_{ij} is the component in row i and column j of C .

Step 3: Compute $Q_{\text{Sort}} = \text{Sort}([q_1, q_2, \dots, q_n] | [s_1, s_2, \dots, s_n])$, where $\text{Sort}(A|B)$ is a function that sorts the components of A based on the scores in B .

Output: Bag = Top- $r\%$ (Q_{Sort}).

2.5 Salient instance inference

Given the salient bag derived from the Sii process, we will aggregate the bag using MIL aggregation and finally make WSI-level prediction. The MIL aggregation function we are using is the attention-based MIL (ABMIL) [12].

Given a salient bag $B = \{q_1, \dots, q_t\}$ for a WSI, we have the formulation:

$$z = \sum_i^t a_i q_i \quad (8)$$

where:

$$a_i = \frac{\exp\left(W^T(\tanh(V^T q_i) \odot \text{sigm}(U^T q_i))\right)}{\sum_{j=1}^o \exp\left(W^T(\tanh(V^T q_j) \odot \text{sigm}(U^T q_j))\right)} \quad (9)$$

where $V \in \mathbb{R}^{D \times L}$, $U \in \mathbb{R}^{D \times L}$ and $W \in \mathbb{R}^{L \times D}$ are the learnable weights of fully connection networks. Each instance $q_i \in \mathbb{R}^{D \times 1}$ is scaled by attention weight $a_i \in \mathbb{R}$ and summed to yield the representation vector $z \in \mathbb{R}^{D \times 1}$ for bag B . Finally, we apply a separate fully connection network on to z to make WSI-level prediction. The overview of the complete SiiMIL is shown in Fig. 3.

2.6 Implementation details and evaluation metrics

In data preprocessing stage, we cropped each WSI into 224×224 image patches without overlapping under $20 \times$ magnification. We applied color thresholding method to extract foreground tissue patches and discarded background patches that contained less than 75% foreground tissue. Then, we embedded each patch with a ResNet50 model [22] pre-trained on ImageNet dataset [23]. The ResNet50 was truncated after the third residual block which embedded patches into 1024-dimension feature embeddings.

During the training of our MIL model, we used Adam Optimizer [24] with 0.0002 learning rate and 0.00001 weight decay. To avoid overfitting, we applied early stopping strategy with the patience of 10 epochs and the maximum training of 100 epochs depending on the validation loss. In other words, the training was halted if the validation loss do not decrease for 10 epochs.

We conducted five-fold cross-validation on the training set with random splits in the ratio of training: validation set = 90:10. Then, we selected the model with the best validation AUC and evaluated it on the official testing set of Camelyon16. Our model contained three primary hyperparameters: t_i , K and r . To clarify, t_i controls how many representative instances that we select from each normal WSI using CUR-decomposition, K controls the top_K operator during the cosine similarity comparison, and r controls the top- $r\%$ salient instances selection. We tuned and selected the hyperparameters based on the validation AUC and decided to choose $t_i = 100$, $K = 150$, and $r = 0.3$.

We used five evaluation metrics to evaluate the WSI-level classification performance, which are accuracy, AUC (of ROC), precision, recall, and F1-score. Moreover, to evaluate the effect of Sii module, we defined the metric “tumor instance rate” (TIR) as:

$$TIR = \frac{\text{Number of tumor instances}}{\text{Numer of all instances}} \quad (8)$$

for a bag of instances.

Our code is available at: <https://github.com/JoeSu666/SiiMIL>

3 RESULTS

In this section, we demonstrate the experimental results of our method along with the comparison with existing methods. In addition, we exhibit the ablation study results and interpretability of our SiiMIL.

3.1 Results of tumor instance inference

To validate the effectiveness of Salient instance embeddings inference, we grouped the WSIs based on their TIR in four groups: (i) $< 0.5\%$, (ii) $0.5\%-1\%$, (iii) $1\%-10\%$, (iv) $\geq 10\%$. In Fig. 4, we exhibited the performance of salient instance inference across different groups by comparing the TIR of original tumor WSIs and the tumor bags after applying Sii.

3.2 Results on WSI classification

In Table 1, we presented our performance on Camelyon16 dataset and compared them with a set of state-of-the-arts deep learning-based MIL models [9, 10, 12, 13]. The proposed SiiMIL achieved 0.9225 AUC which outperforms the comparison models. To be noticed, the ABMIL was the baseline method of SiiMIL that didn't perform Sii and applied the attention module to all the instances of the WSIs. We observed more than 8% improvement in AUC from the baseline to our SiiMIL.

Due to the remarkable bag TIR improvement by using the Sii, our SiiMIL also achieved outstanding recall compared to the comparison methods, which is crucial in medical domain. To demonstrate the effect of tumor instance rate on recall, we grouped the tumor WSIs in different TIRs: (i) $< 0.5\%$, (ii) $0.5\%-1\%$, (iii) $1\%-10\%$, (iv) $\geq 10\%$. Then, we evaluated the MIL models' recall in every group of tumor WSIs (see Fig. 5). Here, we compared the MIL models that used the same aggregation function (i.e. attention-based aggregation).

3.3 Salient instance inference as an addition to MIL models

Other than an integrated MIL model, our Sii module can be also treated as a powerful addition to other MIL models. In Table 2, we presented the performance of some MIL models that used ResNet50 feature extractor as our model did. In parallel, we presented their performance where we applied Sii to form bags before MIL process. We observed that, by feeding salient bags yielded by our Sii, all methods achieved improved performance with significance.

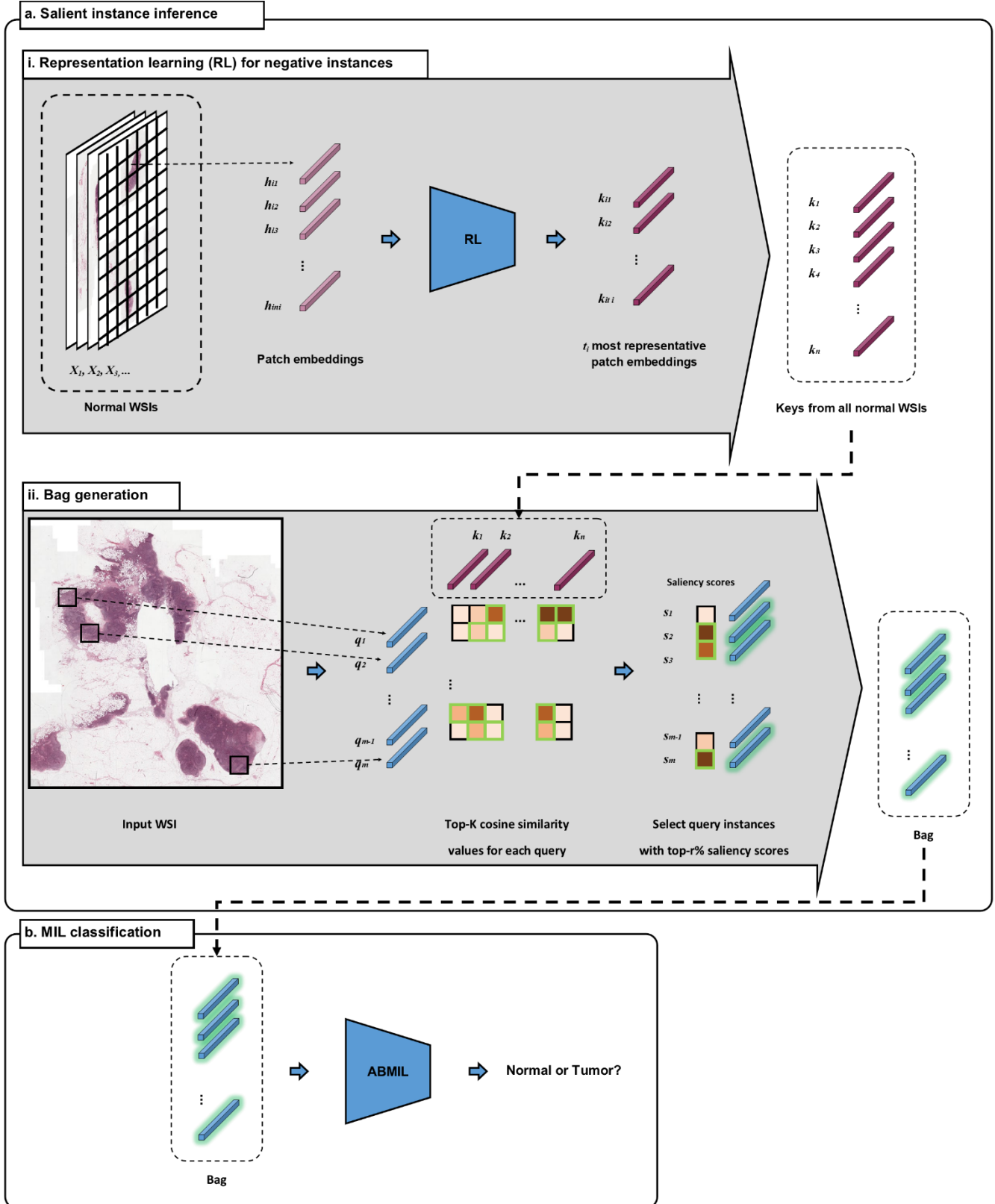


Fig. 3. Overview of our SiIMIL. Our model is comprised of two main steps: (a) salient instance inference, and (b) MIL classification. For the salient instance inference, (a.i) we first learn the representative normal patch embeddings, which we call keys, from all normal WSIs. (a.ii) Then, given an input WSI, we compare every instance with the keys, and select a bag of salient instances as the representation for the given WSI. (b) Finally, we use attention-based MIL to predict the bag.

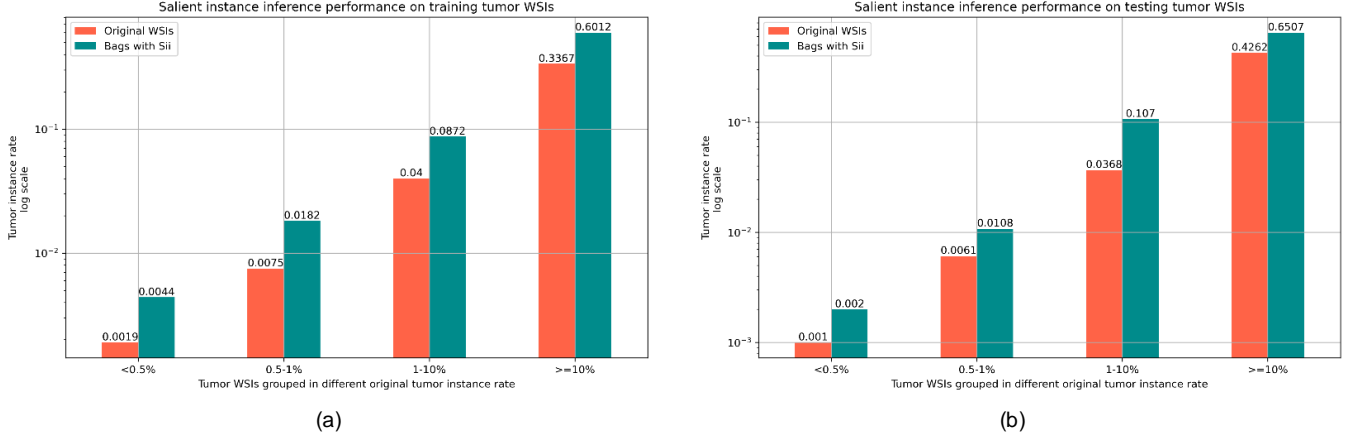


Fig. 4. Performance of Sii module on the tumor WSIs of Camelyon16 dataset. The tumor instance rate was used as an evaluation metric. We compared the TIR of original tumor WSIs, where all the instances in a WSI form a bag, with the TIR of corresponding WSIs after Sii. The WSIs are divided into different groups according to their original TIRs. (a) Sii performance on training tumor WSIs. (b) Sii performance on testing tumor WSIs.

TABLE 1

CLASSIFICATION RESULTS ON CAMELYON16 DATASET WITH 95% CI [LL, UL]

Methods	AUC	Accuracy	Precision	Recall	F1-score
ABMIL [12]	0.8375 [0.8349, 0.8419]	0.8372 [0.8353, 0.8404]	0.8684 [0.8668, 0.8759]	0.6734 [0.6695, 0.6802]	0.7586 [0.7530, 0.7612]
CLAM [13]	0.8319 [0.8298, 0.8367]	0.8295 [0.8274, 0.8326]	0.8462 [0.8380, 0.8475]	0.6735 [0.6682, 0.6791]	0.7500 [0.7440, 0.7524]
DSMIL [9]	0.8265 [0.8219, 0.8281]	0.7907 [0.7886, 0.7939]	1.0000 [1.0000, 1.0000]	0.4490 [0.4429, 0.4540]	0.6197 [0.6086, 0.6193]
TransMIL [10]	0.8926 [0.8889, 0.8939]	0.8759 [0.8723, 0.8768]	0.9714 [0.9693, 0.9739]	0.6938 [0.6862, 0.6967]	0.8095 [0.8021, 0.8098]
SiiMIL	0.9225 [0.9202, 0.9243]	0.8915 [0.8895, 0.8938]	0.9487 [0.9463, 0.9518]	0.7551 [0.7497, 0.7596]	0.8409 [0.8349, 0.8417]

Note. LL and UL represent the lower-limit and upper-limit of the 95% CI.

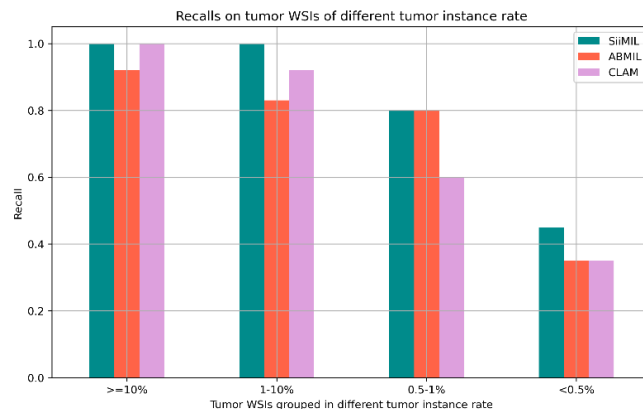


Fig. 5. Classification recall on tumor WSIs grouped in different TIRs.

3.4 Ablations studies

We further conducted ablation studies to investigate the

effects of three primary hyperparameters to our model: t_i , k , and r . To investigate the effect of numbers of CUR-based keys, we created key sets by setting $t_i = 50, 100, 200, 300$ and 400 , and named the derived key sets as: (i) CUR-50, (ii) CUR-100, (iii) CUR-200, (iv) CUR-300, and (v) CUR-400. Then, we applied those key sets separately in our SiiMIL and evaluated the resulted mean validation AUCs based on a five-fold cross-validation. From Fig. 6a, we found that our method achieved best performance when we used the CUR-100 key sets.

In Fig. 6b, we presented the mean validation AUCs of our method when we used different (k, r) settings. We observed that our method achieved the best performance when we chose $k = 150$ and $r = 0.3$.

TABLE 2
PERFORMANCE OF SII AS AN ADDITION TO OTHER MIL MODELS WITH 95% CI

Methods	AUC	Accuracy
ABMIL [12]	0.8375 [0.8349, 0.8419]	0.8372 [0.8353, 0.8404]
Sii+ABMIL	0.9225 [0.9202, 0.9243]	0.8915 [0.8895, 0.8938]
CLAM [13]	0.8319 [0.8298, 0.8367]	0.8295 [0.8274, 0.8326]
Sii+CLAM	0.8747 [0.8711, 0.8772]	0.8527 [0.8494, 0.8543]

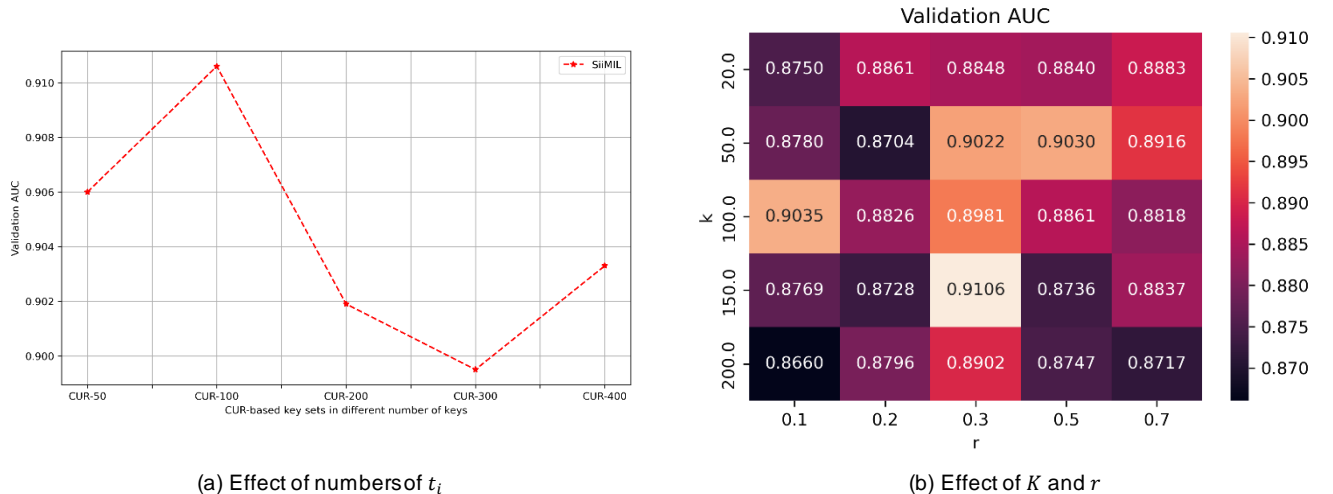


Fig. 6. Ablation study on hyperparameters. (a) Effect of numbers of CUR-based keys. (b) Effect of K and r . All metrics in the figures were the averaged validation AUCs based on the five-fold cross-validation results.

3.5 Interpretability of SiiMIL

Fig. 7 depicts a normal WSI as well as the position of the representative negative instances (keys). Fig. 7a depicts a typical WSI from our dataset. The location of the 100 keys selected by the proposed representation learning methodology are depicted in Fig. 7b. It is clear that these 100 keys correspond to different anatomical structures within the example WSI. Fig. 7c depicts a heatmap in which each instance embedding is colored the same as its most similar key (measured using cosine similarity in the feature space).

Our SiiMIL is also of high interpretability which is important for a diagnostic tool. To demonstrate the interpretability of SiiMIL, we visualized some small tumor WSIs' attention heatmaps that produced by the attention module of our model in Fig. 8 (middle column). As comparison, we also visualize the corresponding attention heatmaps produced by the MIL model without using our Sii (i.e., original attention-based MIL) in Fig. 8 (right column). In the heatmaps, the regions with high brightness correspond to

the instances that received high attention weights. We can clearly observe that the SiiMIL is sensitive to the tumor regions during predictions, even on the small tumor WSIs.

4 DISCUSSION

In this study, we develop a novel salient instance inference-based multiple instance learning algorithm for WSI classification. Our contributions are twofold: (i) we develop a CUR-based representation learning method to mine the representative negative instances from negative bags (i.e., normal WSIs); (ii) we develop a salient instance inference method that can effectively select salient instances (i.e., possible positive instances) from a WSI so that we can form a bag by collecting salient instances only and feed our MIL model with this easy-to-classify bag.

The primary concept behind our method is that feeding MIL models with the salient instances only, instead of feeding all instances, can yield an easier classification problem. To achieve this goal, we propose salient instance inference (Sii) where we innovatively infer salient instances by comparing similarities between incoming instances and the rep-

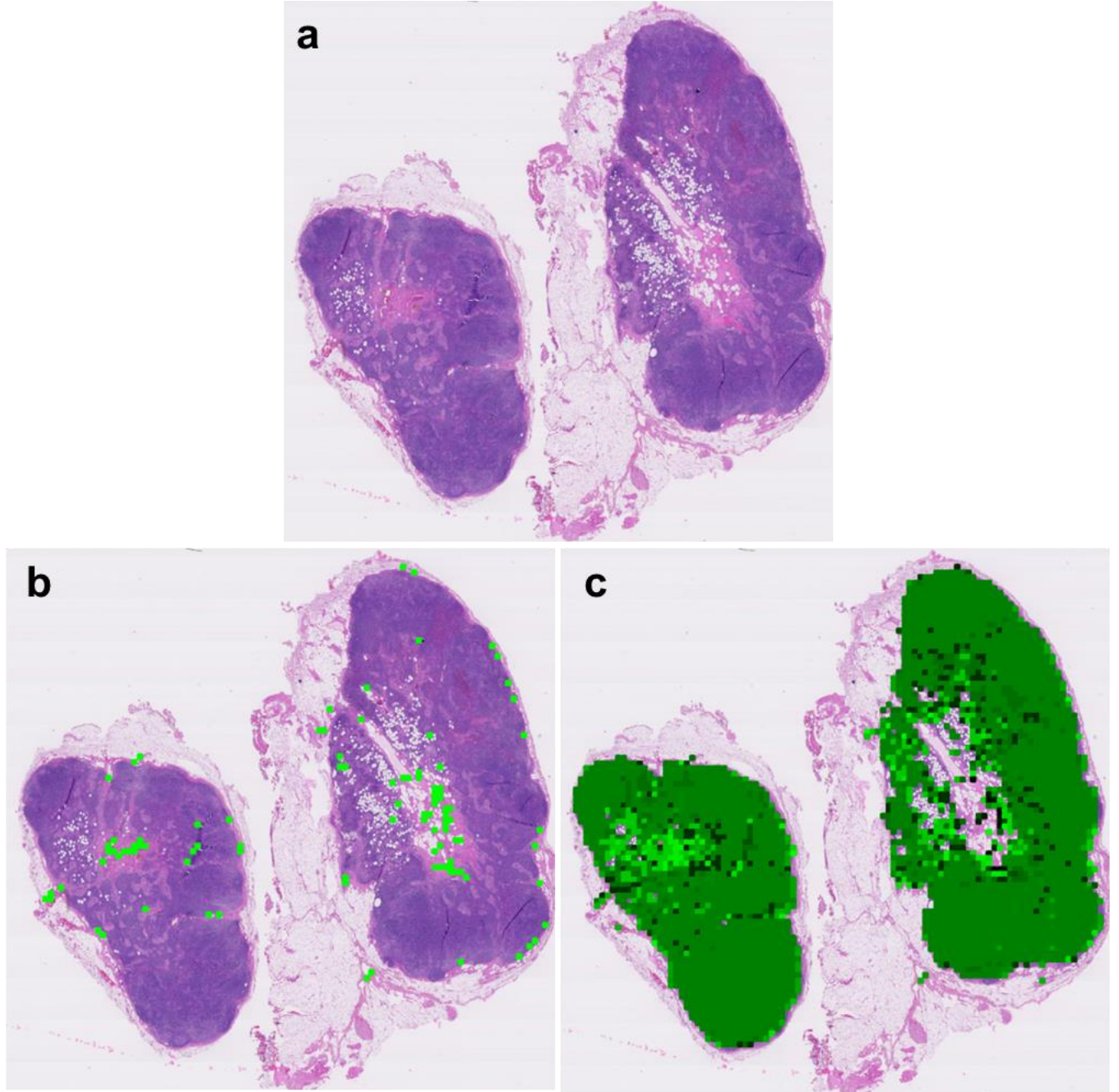


Fig. 7. Visualization of keys from a normal WSI. a) An example of a normal WSI. (b) The placement of the keys on top of the normal WSI. Each green block represents one of the 100 keys learned from the WSI. (c) Patch colormap, where patches of the same color share the same key representation.

representative negative instances. This idea is inspired by the open-set learning [25, 26] and anomaly detection [17, 27] technologies. Under the open-set learning and anomaly detection context, we need first to learn data representations from a set of labeled seen data and then reject the incoming data from unseen categories. This scenario naturally fits the WSI classification problems since hospitals usually have abundant normal WSIs whose local image patches can all be labeled as normal without dedicated delineation. Therefore, in our method, we first conduct a semi-supervised represen-

tation learning on the instances from the normal WSIs using CUR decomposition. To the best of our knowledge, this is the first study of using CUR to learn representations for the WSIs. After learning a strong set of “key” negative instances, given a query WSI, we proposed a transformer-like architecture [21, 28] to compare cosine similarities between the query instances and the keys. Leveraging the difference between negative and positive patterns, we hence infer the most dissimilar query instances and claim them as salient instances.

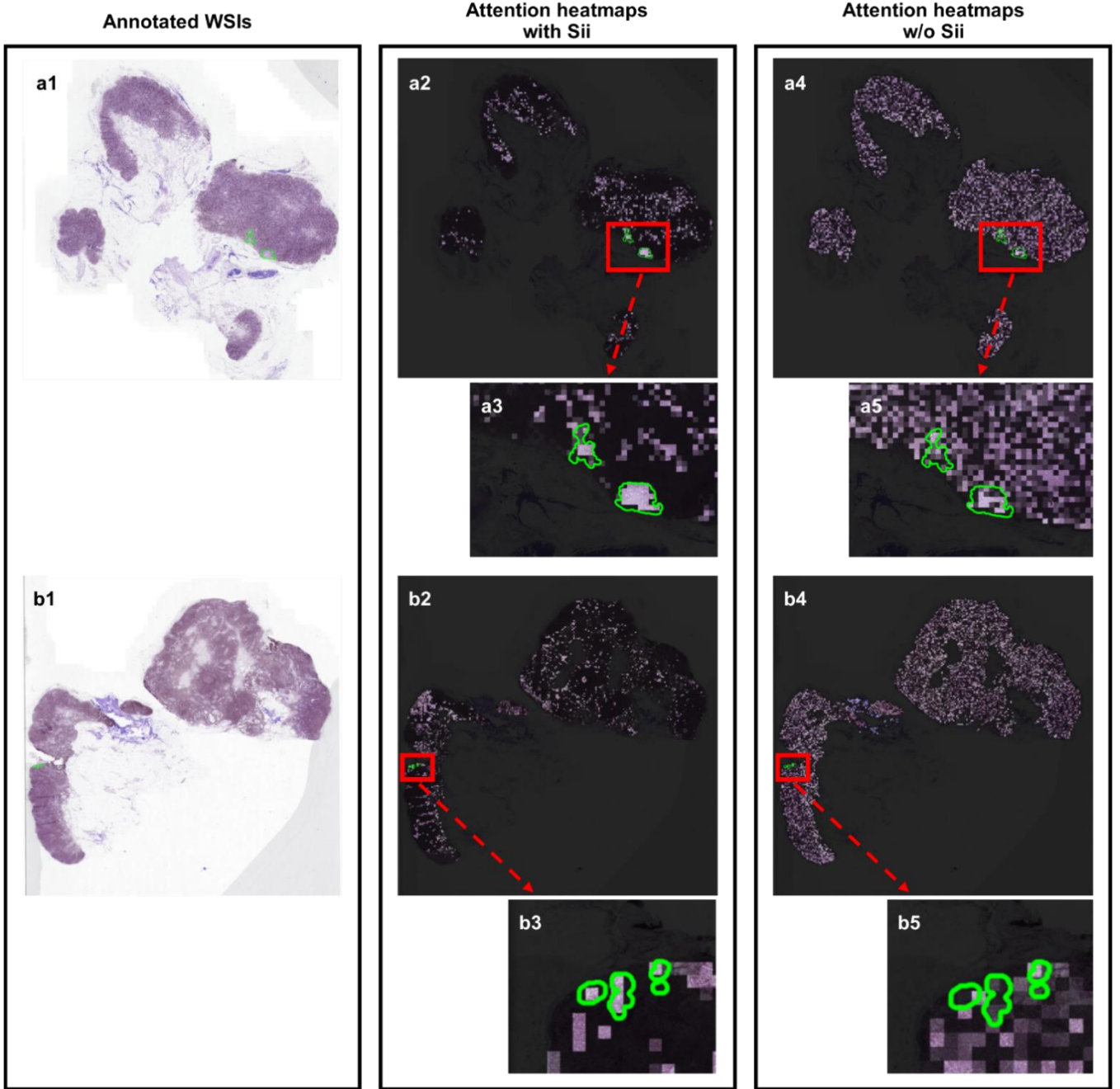


Fig. 8. Attention heatmaps visualization for example small tumor WSIs. The middle column shows the heatmaps produced by our Sii MIL. As comparison, the right column shows the heatmaps produced by the MIL model without using Sii. The attention weight of each patch is assigned by the attention module of the MIL models. Here, we visualize the weights onto the corresponding patches of the WSIs, so that the brighter regions are corresponding to the instances with high attention weights. The attention weights are scaled within 0-1 to enhance the contrast for visibility purpose.

By applying our Sii module to the tumor WSIs, we effectively improve the TRIs of the resulting bags in two to four times compared to the TRIs of the original WSIs. Notably, we achieve this level of improvement even on the tumor WSIs whose original TRIs are lower than 1%, which are extremely difficult cases for the WSI classification problem. Based on the effectiveness of Sii, our SiiMIL achieves an AUC of 0.9225 (95% CI: [0.9202, 0.9243]) and an accuracy of 0.8915 (95% CI: [0.8895, 0.8938]), which outperforms the

state-of-the-art MIL models. Since there is no overlap between the AUC's confidence intervals of our method and the comparison methods, we conclude that our SiiMIL outperforms the state-of-the-art MIL methods significantly. In addition, we show that existing MIL models' performance in terms of recall will decrease with decreasing TRIs of the WSIs (see Fig. 5). This observation verifies our motivation of improving the positive instance rate (see Section 2.2 for details). Despite declining TRIs, SiiMIL still outperforms previ-

ous MIL models in recall, further supporting our suggestion to raise the positive instance rate. Our Sii is also a powerful addition to the existing MIL models. In Table 2, we exhibit that our Sii improves the AUCs of two existing MIL models by 4-9%. Lastly, our SiiMIL method has excellent interpretability. From the attention heatmaps shown in Fig. 8, we can clearly observe that our model accurately pays attention to the tumor regions during predictions, even on the small tumor WSIs.

The main limitation of our method lies in the fact that it only fits the conventional present-or-not MIL scenario. In the WSI classification context, there needs to be an exclusive type of target tissue that only exists in the positive WSIs, such as tumors or other lesions. Our Sii will fail in the scenario when both negative and positive WSIs are composed of multi-types of tissues, and we need to make predictions by analyzing different types simultaneously, such as Gleason score prediction [29], cancer recurrence prediction [30], etc.. To solve the problems in the second scenario, we need to come up with a different type of instance selection strategy which can analyze the distributions of different tissue types [16].

Our method can also be improved by taking the contextual information into account in the MIL aggregation stage [10, 31]. However, since we omit 70% of the instances using our Sii, we cannot simply apply our method to the existing context-based MIL models. Instead, we can develop special position encoding methods for our Sii to fit those models. Lastly, in the future, we will try to make our Sii module trainable and train together with the MIL module so that we can learn better salient instance inference strategy constrained by the classification loss function.

In spite of the limitations, our SiiMIL is an innovative and effective model for the WSI classification task. In addition, our Sii method creates a new paradigm that different negative instance representation learning method can be explored and applied to our method for better salient instance inference outcomes. Moreover, we believe that our idea about instance selection for MIL models will trigger more discussion on how to improve the performance of MIL models by selecting instances. Finally, the proposed Sii method can be also applied in the WSI image retrieval task, which is a hot topic recently [32, 33]. Briefly, our CUR-based representation learning can be used as a database generation method, and our similarity comparison strategy can be used as the image retrieval method in the WSI image retrieval context.

5 CONCLUSIONS

In conclusion, we proposed a salient instance inference based multiple instance learning model that can accurately classify WSIs. The proposed method achieved excellent accuracy in predicting breast cancer metastasis to lymph node with outstanding recall, even for the WSIs with extremely small tumor regions. Our study also provides possible directions for the future MIL and WSI classification study. We believe that our SiiMIL will be an accurate automatic diag-

nosis tool with strong recall and clinical interpretability. In the long term, our method could yield multiple successful applications in different medical scenarios and therefore improve the clinical diagnosis.

ACKNOWLEDGMENT

The work was partly supported through a National Institutes of Health Trailblazer award R21EB029493 (PIs: Niazi, Segal). The content is solely the responsibility of the authors and does not necessarily represent the official views of the National Institutes of Health.

REFERENCES

- [1] M. N. Gurcan, L. E. Boucheron, A. Can, A. Madabhushi, N. M. Rajpoot, and B. Yener, "Histopathological image analysis: A review," *IEEE reviews in biomedical engineering*, vol. 2, pp. 147-171, 2009.
- [2] M. K. K. Niazi, A. V. Parwani, and M. N. Gurcan, "Digital pathology and artificial intelligence," *The lancet oncology*, vol. 20, no. 5, pp. e253-e261, 2019.
- [3] A. Esteva *et al.*, "Deep learning-enabled medical computer vision," *NPJ digital medicine*, vol. 4, no. 1, pp. 1-9, 2021.
- [4] N. Kumar, R. Verma, S. Sharma, S. Bhargava, A. Vahadane, and A. Sethi, "A dataset and a technique for generalized nuclear segmentation for computational pathology," *IEEE transactions on medical imaging*, vol. 36, no. 7, pp. 1550-1560, 2017.
- [5] S. Wang *et al.*, "RMDL: Recalibrated multi-instance deep learning for whole slide gastric image classification," *Medical image analysis*, vol. 58, p. 101549, 2019.
- [6] S. Graham *et al.*, "Hover-net: Simultaneous segmentation and classification of nuclei in multi-tissue histology images," *Medical Image Analysis*, vol. 58, p. 101563, 2019.
- [7] D. Wang, A. Khosla, R. Gargya, H. Irshad, and A. H. Beck, "Deep learning for identifying metastatic breast cancer," *arXiv preprint arXiv:1606.05718*, 2016.
- [8] G. Campanella *et al.*, "Clinical-grade computational pathology using weakly supervised deep learning on whole slide images," (in English), *Nat Med*, vol. 25, no. 8, pp. 1301-+, Aug 2019, doi: 10.1038/s41591-019-0508-1.
- [9] B. Li, Y. Li, and K. W. Eliceiri, "Dual-stream multiple instance learning network for whole slide image classification with self-supervised contrastive learning," in *Proceedings of the IEEE/CVF Conference on Computer Vision and Pattern Recognition*, 2021, pp. 14318-14328.
- [10] Z. Shao, H. Bian, Y. Chen, Y. Wang, J. Zhang, and X. Ji, "Transmil: Transformer based correlated multiple instance learning for whole slide image classification," *Advances in Neural Information Processing Systems*, vol. 34, pp. 2136-2147, 2021.
- [11] X. Wang, Y. Yan, P. Tang, X. Bai, and W. Liu, "Revisiting multiple instance neural networks," *Pattern Recognition*, vol. 74, pp. 15-24, 2018.
- [12] M. Ilse, J. Tomczak, and M. Welling, "Attention-based deep multiple instance learning," in *International conference on machine learning*, 2018: PMLR, pp. 2127-2136.

[13] M. Y. Lu, D. F. Williamson, T. Y. Chen, R. J. Chen, M. Barbieri, and F. Mahmood, "Data-efficient and weakly supervised computational pathology on whole-slide images," *Nature biomedical engineering*, vol. 5, no. 6, pp. 555-570, 2021.

[14] P. Courtiol, E. W. Tramel, M. Sanselme, and G. Wainrib, "Classification and disease localization in histopathology using only global labels: A weakly-supervised approach," *arXiv preprint arXiv:1802.02212*, 2018.

[15] N. Coudray *et al.*, "Classification and mutation prediction from non-small cell lung cancer histopathology images using deep learning," *Nat Med*, vol. 24, no. 10, pp. 1559-1567, 2018.

[16] Z. Su, T. E. Tavolara, G. Carreno-Galeano, S. J. Lee, M. N. Gurcan, and M. K. K. Niazi, "Attention2majority: Weak multiple instance learning for regenerative kidney grading on whole slide images," *Med Image Anal*, vol. 79, p. 102462, Jul 2022, doi: 10.1016/j.media.2022.102462.

[17] C. Ding, G. Pang, and C. Shen, "Catching Both Gray and Black Swans: Open-set Supervised Anomaly Detection," in *Proceedings of the IEEE/CVF Conference on Computer Vision and Pattern Recognition*, 2022, pp. 7388-7398.

[18] B. E. Bejnordi *et al.*, "Diagnostic assessment of deep learning algorithms for detection of lymph node metastases in women with breast cancer," *Jama*, vol. 318, no. 22, pp. 2199-2210, 2017.

[19] M. W. Mahoney and P. Drineas, "CUR matrix decompositions for improved data analysis," *Proceedings of the National Academy of Sciences*, vol. 106, no. 3, pp. 697-702, 2009, doi: doi:10.1073/pnas.0803205106.

[20] P. Drineas, M. W. Mahoney, and S. Muthukrishnan, "Relative-error CUR matrix decompositions," *SIAM Journal on Matrix Analysis and Applications*, vol. 30, no. 2, pp. 844-881, 2008.

[21] A. Vaswani *et al.*, "Attention is all you need," *Advances in neural information processing systems*, vol. 30, 2017.

[22] K. He, X. Zhang, S. Ren, and J. Sun, "Deep residual learning for image recognition," in *Proceedings of the IEEE conference on computer vision and pattern recognition*, 2016, pp. 770-778.

[23] J. Deng, W. Dong, R. Socher, L.-J. Li, K. Li, and L. Fei-Fei, "Imagenet: A large-scale hierarchical image database," in *2009 IEEE conference on computer vision and pattern recognition*, 2009: Ieee, pp. 248-255.

[24] D. P. Kingma and J. Ba, "Adam: A method for stochastic optimization," *arXiv preprint arXiv:1412.6980*, 2014.

[25] K. Cao, M. Brbic, and J. Leskovec, "Open-World Semi-Supervised Learning," in *International Conference on Learning Representations*, 2021.

[26] C. Geng, S.-j. Huang, and S. Chen, "Recent advances in open set recognition: A survey," *IEEE transactions on pattern analysis and machine intelligence*, vol. 43, no. 10, pp. 3614-3631, 2020.

[27] G. Pang, C. Shen, L. Cao, and A. V. D. Hengel, "Deep learning for anomaly detection: A review," *ACM Computing Surveys (CSUR)*, vol. 54, no. 2, pp. 1-38, 2021.

[28] A. Dosovitskiy *et al.*, "An Image is Worth 16x16 Words: Transformers for Image Recognition at Scale," in *International Conference on Learning Representations*, 2020.

[29] M. K. K. Niazi *et al.*, "Visually meaningful histopathological features for automatic grading of prostate cancer," *IEEE journal of biomedical and health informatics*, vol. 21, no. 4, pp. 1027-1038, 2016.

[30] J. Whitney *et al.*, "Quantitative nuclear histomorphometry predicts oncotype DX risk categories for early stage ER+ breast cancer," *BMC cancer*, vol. 18, no. 1, pp. 1-15, 2018.

[31] A. Myronenko, Z. Xu, D. Yang, H. R. Roth, and D. Xu, "Accounting for dependencies in deep learning based multiple instance learning for whole slide imaging," in *International Conference on Medical Image Computing and Computer-Assisted Intervention*, 2021: Springer, pp. 329-338.

[32] X. Wang *et al.*, "RetCCL: clustering-guided contrastive learning for whole-slide image retrieval," *Medical Image Analysis*, vol. 83, p. 102645, 2023.

[33] C. Chen, M. Y. Lu, D. F. Williamson, T. Y. Chen, A. J. Schaumberg, and F. Mahmood, "Fast and scalable search of whole-slide images via self-supervised deep learning," *Nature Biomedical Engineering*, pp. 1-15, 2022.